İSTANBUL TECHNICAL UNIVERSITY ★ INSTITUTE OF SCIENCE AND TECHNOLOGY

NUMERICAL SIMULATION OF NONLINEAR WAVE PROPAGATION IN BUBBLY LIQUIDS

M. Sc. Thesis by

Sarper ARÜN, Aeronautical Engineer

Department : Interdisciplinary Programs

Program: Aerospace Engineering

MAY 2006

İSTANBUL TECHNICAL UNIVERSITY ★ INSTITUTE OF SCIENCE AND TECHNOLOGY

NUMERICAL SIMULATION OF NONLINEAR WAVE PROPAGATION IN BUBBLY LIQUIDS

M. Sc. Thesis by

Sarper ARÜN, Aeronautical Engineer

511031024

Date of submission : 18 April 2006

Date of defence examination: 22 May 2006

Supervisor (Chairman): Prof. Dr. Can Fuat DELALE

Members of the Examining Committee Prof. Dr. Cihat BAYTAŞ

Prof. Dr. Erkan AYDER

MAY 2006

İSTANBUL TEKNİK ÜNİVERSİTESİ ★ FEN BİLİMLERİ ENSTİTÜSÜ

KABARCIKLI SIVILARDA NONLİNEER DALGA YAYILIMININ SAYISAL BENZETİMİ

YÜKSEK LİSANS TEZİ

Uçak Müh. Sarper ARÜN
511031024

Tezin Enstitüye Verildiği Tarih : 18 Nisan 2006
Tezin Savunulduğu Tarih : 22 Mayıs 2006

Tez Danışmanı : Prof. Dr. Can Fuat DELALE
Diğer Jüri Üyeleri Prof. Dr. Cihat BAYTAŞ
Prof. Dr. Erkan AYDER

MAYIS 2006

PREFACE

This thesis is based upon studies performed during September 2003 to April 2006 at the Aerospace Program of Institute of Science and Technology at Istanbul Technical University. In this study, I studied about the numerical simulations of nonlinear wave propagation in bubbly liquids with front tracking method. My graduation project was about bubble dynamics, and I have started to be interested in numerical solutions of flows in bubbly liquids after graduation. The front tracking method makes the numerical analysis of multiphase flows very practical. I used the code which is developed by the group of Prof. Grétar Tryggvason.

I would like to thank my supervisor Prof. Dr. Can Fuat Delale for his advice and guidance during the completion of this thesis. I am most grateful to him for introducing me into this interesting field. I also wish to thank Assistant Prof. Dr. Selman Nas for helping me learn about the solver.

MAY 2006 SARPER ARÜN

TABLE OF CONTENTS

LIST OF FIGURES **v**
LIST OF SYMBOLS **vi**
ÖZET **vii**
SUMMARY **viii**

1. INTRODUCTION **1**

2. PROPAGATION OF SHOCK WAVES IN BUBBLY LIQUIDS **3**
2.1. Bubbly Liquids 3
2.2. Shock Waves in Bubbly Liquids 3

3. FRONT TRACKING METHOD **8**
3.1. General 8
3.2. Governing Equations 9
3.3. The Computational Algorithm 10

4. RESULTS AND DISCUSSION **12**
4.1. Two-Dimensional Simulations 12
4.1.1. Collapse of a Single Vapor Bubble 13
4.1.2. Shock Propagation in Bubbly Liquids Containing Vapor Bubbles 14
4.1.3. Collapse of a Single Gas Bubble 16
4.1.4. Shock Propagation in Bubbly Liquids Containing Gas Bubbles 17
4.2 Three-Dimensional Simulations for Vapor Bubbles 19

5. CONCLUSION **21**

REFERENCES **22**

LIST OF FIGURES

Page No.

Figure 2.1 : The speed of sound vs. frequency in a bubbly liquid..... 4
Figure 2.2 : Travel of a discontinuity with constant speed in bubbly mixture. 5
Figure 2.3 : Characteristic waveforms for *A*, *B* and *C*-type shocks..... 6
Figure 3.1 : Front representation by marker points..... 11
Figure 4.1 : Solution of a single vapor bubble in a two dimensional, rectangular domain by front tracking/finite difference method..... 13
Figure 4.2 : Solution for the propagation of nonlinear pressure waves in a 2D rectangular domain of a bubbly mixture containing 12 vapor bubbles by front tracking/finite difference method..... 14
Figure 4.3 : Pressure distributions for the propagation of nonlinear pressure waves in a 2D rectangular domain of a bubbly mixture containing 12 vapor bubbles..... 15
Figure 4.4 : Solution of a single gas bubble in a two dimensional, rectangular domain by front tracking/finite difference method..... 16
Figure 4.5 : Solution for the propagation of nonlinear pressure waves in a 2D rectangular domain of a bubbly mixture containing 12 gas bubbles by front tracking/finite difference method..... 17
Figure 4.6 : Pressure distributions for the propagation of nonlinear pressure waves in a 2D rectangular domain of a bubbly mixture containing 12 gas bubbles..... 18
Figure 4.7 : Results of shock propagation in a 3D rectangular domain of a bubbly mixture containing 16 spherical vapor bubbles..... 19

LIST OF SYMBOLS

β	: Void fraction
β_0, β_1	: Void fractions behind and in front of a shock
γ	: Polytropic index
Δp	: Pressure jump
D	: Deformation tensor
F_σ	: Body forces (gravity, electromagnetic forces, buoyancy etc.)
L	: Characteristic length
μ	: Viscosity
μ_b	: Viscosity of gas
μ_l	: Viscosity of liquid
n	: Iteration step for discretized equations
p	: Pressure
p_0, p_1	: Pressures behind and in front of a shock
ρ	: Density of bubbly liquid mixture
ρ_b	: Density of gas
ρ_l	: Density of liquid
R	: Radius of bubbles
R_0	: Initial radius of bubbles
Re	: Reynolds number
t	: Time
u	: Shock induced velocity, velocity field
u^*	: Temporary velocity field
U_s	: Propagation speed of a shock wave
x, y, z	: Field point in a fixed grid
x'	: Transformed coordinate of fluid particle
∇_h	: Gradient operator

KABARCIKLI SIVILARDA NONLİNEER DALGA YAYILIMININ SAYISAL BENZETİMİ

ÖZET

Bu çalışmada nonlineer basınç dalgalarının kabarcıklı sıvılarda yayılmasının sonlu hacim/cephe izleme yöntemiyle doğrudan sayısal benzetimi incelenmektedir. Dikdörtgensel bir bölge içerisinde sıkıştırılamaz sıvı ve küresel (2-boyutta silindirik) buhar veya gaz kabarcıkları ele alınmaktadır. Bölgeye üst kenarından sürekli bir basınç uygulanması itibariyle şok dalgasının ilerlemesi incelenmektedir. Diğer matematiksel yaklaşımların aksine, burada göz önünde bulundurulan en önemli husus, kabarcıkların küresel olmayan şekillerde büzülmesinin ve kabarcıkların birbirleriyle ve akış alanıyla olan etkileşimlerinin dikkate alınmasıdır. Benzetimlerin ağ analizi yapılıp, sonuçlar 1-boyutlu homojen kabarcıklı sıvı teorisiyle karşılaştırılmıştır. Basınç grafiğindeki salınımlar akışta süreklilik bulunmadığını gösterse de elde edilen şok hızı değerleri klasik teoriyle benzerlik göstermektedir. Buhar kabarcıklarının olduğu sıvıda bu salınımlar gaz kabarcıklarının bulunduğu sıvıya göre daha belirgindir. Buhar kabarcıklarının bulunduğu kabarcıklı sıvı için elde edilen sonuçlar klasik teoriden elde edilen sonuçlardan gaz kabarcıkları içeren kabarcıklı sıvıya göre daha fazla farklılık gösterir. Ayrıca buhar kabarcıklarının iyi çözümlenebilmesi ağ çözünürlüğüne bağlıdır.

NUMERICAL SIMULATION OF NONLINEAR WAVE PROPAGATION IN BUBBLY LIQUIDS

SUMMARY

In this study nonlinear pressure wave propagation in bubbly liquids is investigated by direct numerical simulations using the front tracking/finite volume method. A bubbly liquid composed of spherical (or cylindrical in 2D) gas or vapor bubbles in an incompressible liquid in a rectangular domain is considered. A constant pressure rise is applied from the top of the domain and the propagation of the shock wave is observed. Beyond the many other mathematical approaches, the most important issue of the method is consideration of non-spherical collapses of bubbles and bubble/bubble interactions. A grid study is made for the simulations and the results are compared with one-dimensional homogeneous bubbly liquid theory. The propagation speeds of shock waves are in agreement with classical theory even though the fluctuations of pressure fields point out that the propagation is not steady. There are more significant fluctuations of pressure field for the bubbly liquid that contains vapor bubbles compared to the one with gas bubbles. The results for the bubbly liquid composed of vapor bubbles vary from the classical approach more than the results for the bubbly liquid composed of gas bubbles does. In addition, resolving vapor bubbles is dependent on grid resolution.

1. INTRODUCTION

Bubbly liquids have received great attention as a medium for propagation of waves because of their highly dispersive features. They also provide information about some physical macroscale events like cavitation or oceanic waves. Shock propagation in bubbly liquids has been investigated for its essential role in science and engineering, particularly for its industrial applications in petroleum and hydraulic engineering, microbiological sciences, etc. Model equations have been introduced for shock waves in bubbly liquids taking into account viscous dissipation, acoustic radiation and thermal damping [1-4]. In all of these investigations, the cumulative behavior of the deformation of bubbles has not been accounted for. The deformation of bubbles together with bubble/bubble interactions in the propagation of nonlinear pressure waves are investigated in the work of Delale *et al.* [5] for vapor and gas bubbles by assuming that the liquid is incompressible while the bubbles are compressible. The results of this work were obtained by *Direct Numerical Simulations* (DNS) of Navier-Stokes equations using the front tracking/finite difference method which has been developed by Tryggvason *et al.* [6]. On the other hand, in order to obtain results that can be compared with experiments [4], relaxation effects due to thermal processes and acoustic radiation should be considered. This requires the solution of the energy equation together with the compressible Navier Stokes equations.

The work presented here concentrates on the grid analysis of the DNS by the front tracking method of shock propagation in bubbly liquids based on the work of Delale *et al.* [5]. The simulations are carried out in rectangular domains in two- and three-dimensions. The bubbles are chosen initially to be spherical in 3D or circular in 2D and at rest. The ratios of liquid density to bubble density and liquid viscosity to bubble viscosity are set equal to 10. The results for different grid resolutions are compared with respect to mean shock speeds and pressure fluctuations.

Although the pressure distributions show that the flow is not steady, the mean shock propagation speeds are in agreement with the classical one-dimensional homogenous bubbly flow theory. It has been found that pressure fluctuations and bubble interfaces are better resolved in finer grids; however, the propagation speeds seem to be independent of grid resolutions. Pressure fluctuations are seen to vary much more in bubbly liquids containing vapor bubbles in contrast to those containing gas bubbles as the grid resolution is increased.

2. PROPAGATION OF SHOCK WAVES IN BUBBLY LIQUIDS

2.1 Bubbly Liquids

Bubbly liquids are worthwhile to examine because of their unexpected behavior when they are exposed to pressure waves. In multiphase flows, bubbly liquids are known to exhibit more pronounced compressibility effects compared to other mixtures like suspensions and emulsions. Even a dilute mixture of a few bubbles can cause very dramatic changes in the compressibility of the liquid, affecting its properties [1].

Theoretically, liquids can be taken to be incompressible. This means that any perturbation (pressure wave, shock, etc.) is felt everywhere in the liquid instantaneously. On the other hand, the speed of any pressure wave or speed of sound for the considered medium becomes finite in a bubbly mixture. If a bubbly liquid is made of air bubbles and water, one may get a lower speed of sound than the speed of sound in air [2]. Specifically, sound waves travel at 334 m/s in air at standard atmospheric conditions and approximately at 1500 m/s in water at room temperature. The fascinating truth is that the speed of sound in a bubbly mixture can have values much lower than 334 m/s.

2.2 Shock Waves in Bubbly Liquids

Bubbly liquids can behave as dispersive media. This means a wave packet consisting of simple waves travels with a group velocity while the wave packet spreads as it propagates. It spreads because each simple wave has its own frequency so that the speed of propagation is dependent on the frequencies of traveling waves [7]. Figure 2.1 shows the propagation speed against the disturbing frequencies of waves [9]. The straight line shows the constant propagation speed in pure water around 1500 m/s.

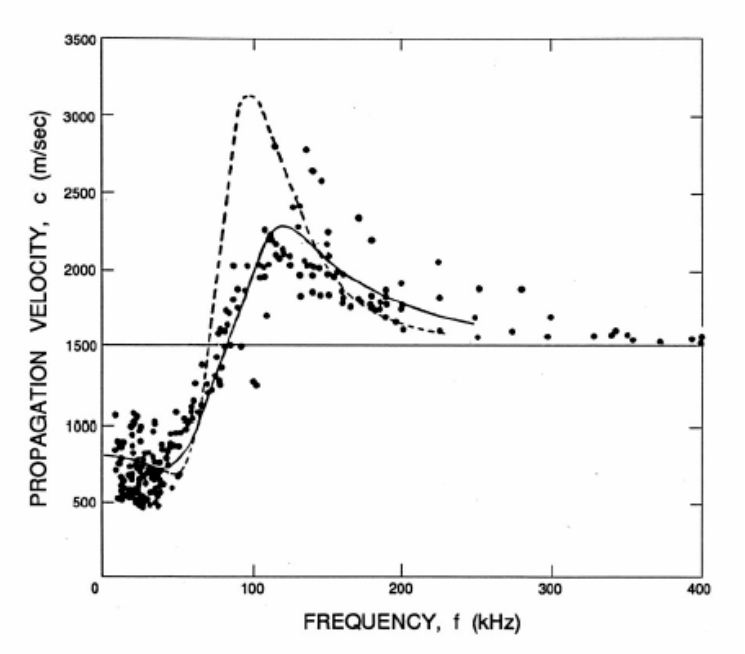

Figure 2.1: The speed of sound vs. frequency in a bubbly liquid†.

The liquid phase is assumed to carry inertial properties of the mixture because the mass of the gas inside the bubbles is negligible. On the other hand, the elasticity of the gas is significant for restoring forces. This may lead to a spring analogy [7], and is helpful for deriving equations for a spherical bubble. When spring analogy is considered, then it is clear that oscillations occur in bubbly liquids. The oscillations are caused by the energy transport between phases [2]. As can be noticed in a bubbly liquid the inertial part (the liquid) contains the potential energy, and the elastic part (the gas) contains the kinetic energy. Refraction, reflection and interference of waves can occur during the propagation of any pressure wave in bubbly liquids. Moreover, the bubbles enforce dynamic boundary conditions for the pressure field where the high pressure is forced to drop to the level stated inside the bubble with liquid inflow into the domain, blocking the propagation of the wave to go further. The latter is the reason why the propagation speed becomes finite in a bubbly liquid, even when the liquid phase itself is taken to be incompressible [5].

In general, the propagation speed in a bubbly liquid depends on the number and the size of the bubbles and on the frequency of the wave [7]. These effects are calculated with the help of the void fraction β (the fraction of gas volume to the volume of the whole mixture). The average density ρ of the mixture can be evaluated as

† Propagation velocity in water which contains air bubbles of radius R_0 = 0.12 mm. and of void fraction β = 0.0002 plotted against frequency. The dots show the experimental data of Fox, Curley, and Larson [9] while the solid line is the fitted distribution to data. The dotted line is from the theoretical results for the mixture of bubbles of R_0 = 0.11 mm [8].

$$\rho = \rho_l(1-\beta) \tag{2.1}$$

where ρ_l denotes the liquid density and where the contribution from the density of the gas is neglected. When considering a steady-state flow between two uniform regions, designated by 0 and 1, separated by a discontinuity (shock wave), a simple relation for the shock speed can be found relating the properties on each side [2]. The shock is assumed to travel with a constant velocity U_s between regions 0 and 1, as shown in fig. 2.2. The pressures and void fractions in the regions are designated by p_0, p_1 and β_0, β_1, respectively.

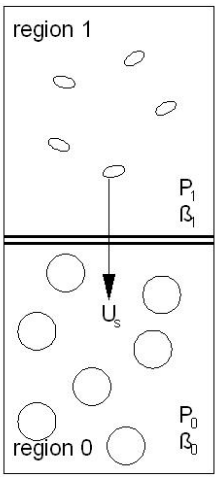

Figure 2.2: Travel of a discontinuity with constant speed in bubbly mixture. The shock wave (double line) separating two uniform regions and traveling with the velocity U_s .

If the continuity equation is transformed to a new frame of x' by the transformation $x' = x + U_s t$, the conservation of mass and momentum in the separated regions yield [3]

$$(1-\beta_1)(U_s + u) = (1-\beta_0)U_s \tag{2.2}$$

and

$$p_0 = p_1 + \rho_l(1-\beta_0)U_s u \quad , \tag{2.3}$$

respectively, where the upstream conditions are designated by subscript 0. Here, u is the shock-induced velocity and is calculated by [3]

$$u = \beta_0 U_s \left(\frac{\beta_1(1-\beta_1)}{\beta_0(1-\beta_0)} - 1 \right) \quad . \tag{2.4}$$

The shock speed U_s of a steady shock wave in a bubbly mixture can be calculated from eq. (2.3) by substituting the shock induced velocity from eq. (2.4) yielding

$$U_s^{\,2} = \frac{(1-\beta_1)(p_0 - p_1)}{(1-\beta_0)(\beta_1 - \beta_0)\rho_l} \quad . \tag{2.5}$$

Equation (2.5) shows that the shock speed U_s in a bubbly mixture depends on the values of the liquid density, the upstream and downstream void fractions and the pressure jump between the upstream and downstream conditions. The equation is derived for uniform regions 0 and 1, separated by a discontinuity, under the assumptions of small void fractions, spherical bubbles and no mass transfer at the interfaces which separate the bubbles and the liquid.

Experiments show that the initial discontinuity in the pressure jump does not remain sharp as it propagates since it dissipates and is dispersed. Noordzij and Wijngaarden [3] find three different steady state shock profiles which they refer to as *A*, *B* and *C*-type shock waves, as shown in fig. 2.3. *A*-type shock waves are usually located near the boundary where the pressure difference is applied. The first profile which shows oscillatory behavior behind the shock is the *A*-type shock wave. For *B*-type waves, thermal and viscous relaxation effects begin to become more effective, making the profile smoother. Finally, *C*-type waves are very smooth and are, therefore, weak shocks.

(a)

(b)

(c)

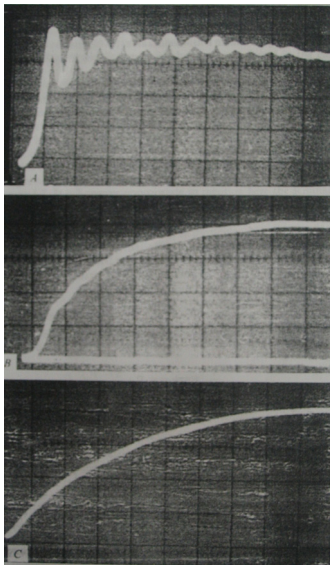

Figure 2.3: Characteristic waveforms for *A*, *B* and *C*-type shocks, observed in the experiments by Noordzij and Wijngaarden in 1974 [3]. (a), (b) and (c) show the cases of *A*-type, *B*-type and *C*-type waves, respectively.

There have been many efforts to create model equations for *A*, *B* and *C*-type waves. Noordzij and Wijngaarden [3] presented models based on relaxation effects due to slip between phases to explain the transition between *A*-, *B*- and *C*-type shocks. Beylich and Gülhan [2] introduced a model for *A*-type shock waves and stated the validity of Wijngaarden's model; however, the results of Watanabe and Prosperetti [1] did not agree with them. Matsumoto *et al.* [4] used model equations similar to Van Wijngaarden's and compared the results with experiments. They found the significance of thermal damping in the simulation as well as the uniformity of the bubbly mixture in the experiments.

The models account for thermal damping, dispersion, viscous dissipation and relaxation, but the most important assumption is that the bubbles are spherical leaving out effects of bubble deformations and bubble/bubble interactions. Direct Numerical Simulations of the full Navier-Stokes equations can provide information on bubble deformations and bubble/bubble interactions. This attempt will be undertaken in the present thesis.

3. FRONT TRACKING METHOD

3.1 General

The front tracking finite difference method is a simulation method used for multiphase flows. Before discussing the characteristic features of the front tracking method, other important simulation techniques that have been used for the simulations of multiphase flows so far should also be mentioned.

There are several methods to numerically simulate multiphase flows [6]. In the front capturing method, the whole flow field is simulated on a regular, stationary grid. There is a need for a marker component in front capturing techniques in order to identify which fluid the considered point is in. In the marker-and-cell method (MAC), massless particles are injected inside the mesh. The trajectories of these particles are tracked. In the volume-of-fluid (VOF) method, volume fractions are advected on the fixed grid for that purpose. Although there are efforts to deal with the difficulties, the main problems people encounter with front capturing methods are the computation of surface tension and difficulty in resolving sharp boundaries smaller than the grid size between two phases.

The second method consists of the technique of using different grids for each phase. The grids are connected to each other at the boundaries. This technique presents the highest accuracy, but is appropriate only for simple geometries.

The Lagrangian methods, in which the fluid is followed by an adaptive grid, constitute another class of techniques for the simulation of multiphase flows. This approach is rather complicated.

Finally in the front tracking method, the interface is traced by connected marker points, but the simulation is done on a fixed grid. When a front is tracked, each phase is treated separately. For the simulations employed here, a regular and staggered grid is used where both phases are treated together [6]. There is only one set of governing equations that are written for the whole domain and discussed in the following section.

3.2 Governing Equations

In the front tracking method, the unsteady Navier-Stokes equations are solved by a conservative finite difference method on a fixed, staggered grid. The interface, called *the front*, is tracked with the help of marker points. The front advects in the fluid and pressure equations are solved for the flow field using the given values of pressure in the bubbles depending on the bubble contents. For the numerical simulation of the problem, the unsteady Navier-Stokes equations are solved for the whole flow field including the liquid and the bubbles [5].

$$\frac{\partial(\rho\mathbf{u})}{\partial t} + \nabla\cdot(\rho\mathbf{u}\mathbf{u}) = -\nabla p + \nabla\cdot(2\mu D) \qquad \textbf{(3.1)}$$

Here **u** denotes the velocity field, p denotes the pressure and D denotes the deformation tensor. The density varies in the interval $\rho_b \le \rho \le \rho_l$ and the viscosity varies in the interval $\mu_b \le \mu \le \mu_l$, where subscripts b and l denote bubble and liquid, respectively. In this simulation, surface tension effects will also be left out.

Another important assumption is about the carrier liquid. The liquid is assumed to be incompressible, satisfying

$$\nabla\cdot\mathbf{u} = 0\,. \qquad \textbf{(3.2)}$$

On the other hand, the bubbles in our simulation are assumed to be compressible. The pressure inside the bubbles is set equal to a constant value or is assumed to change isothermally by assuming a polytropic index γ equal to unity. Thus the pressure inside the bubble is given by

$$p = p_0 \qquad \text{or} \qquad p = p_0\left(\frac{V_0}{V}\right)^{3\gamma} \qquad \textbf{(3.3)}$$

where subscript 0 now refers to the initial values.

3.3 The Computational Algorithm

The front consisting of connected marker points advects and deforms according to the velocity values from DNS, and equations are solved in the domain which contains both fluids separated by the recently advected front.

The numerical simulation is made by a projection method. First, the density field is updated all over the domain using the velocity at the current time step [6].

$$\rho^{n+1} = f(\rho^n, \mathbf{u}^n, \Delta t) \tag{3.4}$$

The expression (3.4) represents an operation that moves the front and then distributes the density values at time step n+1 according to the new layout of the front. After updating the density values, the velocity field can be found all over the domain by solving the Navier-Stokes equations.

First step of solving Navier Stokes equations is called the predictor step. Here, a temporary velocity field $\mathbf{u}^*$ is found by neglecting the pressure gradient. This is done by using a first order, explicit, forward in time scheme as

$$\frac{\rho^{n+1}\mathbf{u}^* - \rho^n\mathbf{u}^n}{\Delta t} = -\nabla_h \cdot \rho^n\mathbf{u}^n\mathbf{u}^n + \nabla_h \cdot \mu^n\left(\nabla_h\mathbf{u}^n + \nabla_h^T\mathbf{u}^n\right) + \mathbf{F}_\sigma \ . \tag{3.5}$$

Here, the left hand side is the discrete form of time derivative. The first term on the right hand side is the advection term, the second is the viscous forces and the last one is the surface tension forces.

In the second step, known as the correction or projection step, the pressure gradient is added, i.e.,

$$\frac{\rho^{n+1}\mathbf{u}^{n+1} - \rho^{n+1}\mathbf{u}^*}{\Delta t} = -\nabla_h P \, . \tag{3.6}$$

Here the subscript h denotes a numerical approximation [6]. In order to determine the pressure in eq. (3.6), the continuity equation is used for eliminating the velocity field at time step n+1.

$$\nabla_h \cdot \mathbf{u}^{n+1} = 0 \, . \tag{3.7}$$

Finally, $\mathbf{u}^{n+1}$ is eliminated from eq. (3.6) with the help of eq. (3.7) resulting in a Poisson equation

$$\nabla_h \cdot \frac{1}{\rho^{n+1}} \nabla_h P = \frac{1}{\Delta t} \nabla_h \cdot \mathbf{u}^* \qquad \textbf{(3.8)}$$

to be solved for the pressure field.

The simulations provide properties on grid points. Since the front moves with the fluid velocities, the velocity of the interface points is found by interpolating the values of the fixed grid. As the front velocity is found, the new position of the front is located by using the same time integration method of the Navier-Stokes equation [6]. The fluid properties do not advect directly. When the front moves, some grid points remain outside the bubble and some don't. After the densities and viscosities are updated according to the new location of the front, the discrete Navier-Stokes equations are solved. If a point is in liquid part, the Poisson equation, eq.(3.8), can be solved for the pressure. This is an iterative process and in the work presented here, is done by a successive over relaxation (SOR) method. If the point is in the area enclosed by the marker points of the interface shown in fig. 3.1, the pressure is calculated iteratively until its value inside the bubble from eq.(3.3) is reached. If there is any surface tension, it is calculated on the interface and the forces are distributed to the neighboring fixed grid points [6]. Finally the velocity field for the new time step is updated by using these data and the procedure given above.

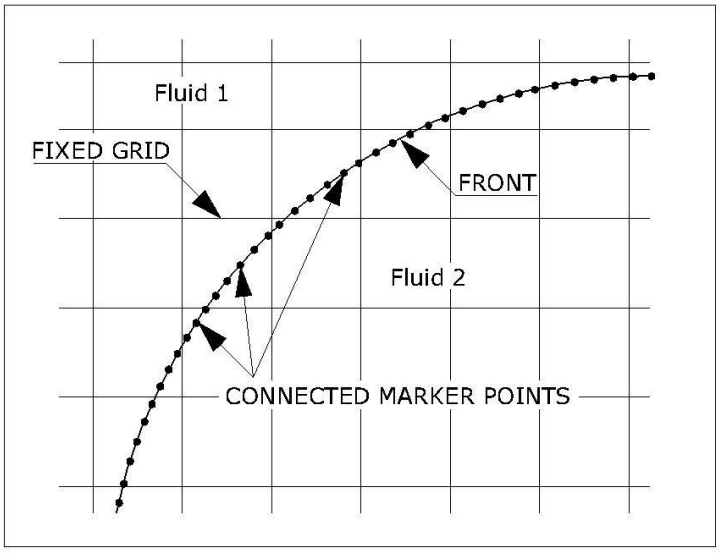

Figure 3.1: Front representation by marker points. The governing equations of multifluid flow computations are solved in a fixed grid while the connected marker points (front) separate two phases [6].

4. RESULTS AND DISCUSSION

The simulation is carried out for a nonlinear pressure wave traveling in a rectangular domain consisting of a bubbly liquid with liquid to bubble density and liquid to bubble viscosity ratios set equal to 10. Initially the bubbles are assumed to be in equilibrium with the surrounding liquid. A wall condition at the end of the tube with no outflow is imposed and periodic conditions are assumed in the transverse directions.

A pressure jump Δp is applied at the top of the domain and is kept constant during the simulations. This causes a liquid inflow at the top resulting in a finite speed of propagation. The liquid in the mixture is taken to be incompressible while the bubbles are compressible (the pressure inside the bubbles is either set equal to a constant or varied isothermally, as in eq.(3.3)). Each simulation corresponds to a fixed Reynolds number given by [5]

$$Re = \frac{\rho_l \sqrt{\Delta p / \rho_l}\, L}{\mu_l} \tag{4.1}$$

where L is the characteristic length of order of the initial mean radius of bubbles and selected as $L = 4R$ in this thesis. Characteristic flow speed is $\sqrt{\Delta p / \rho_l}$. The dimensional quantities of Reynolds number Re, initial void fraction β_0, the ratios ρ_l / ρ_b and μ_l / μ_b can be identified according to eq.(4.1) by using the dimensionless values for the simulations of a bubbly mixture in 2D and 3D domains.

4.1 Two-Dimensional Simulations

First simulations are carried out in a two-dimensional rectangular domain containing a bubbly liquid. A 2 x 8 rectangular domain is represented, respectively, by 18 x 66, 34 x 130 and 66 x 258 grid points and a grid convergence analysis is carried out for vapor or gas bubbles.

4.1.1 Collapse of a Single Vapor Bubble

A single bubble which is initially taken to be in equilibrium with the surrounding liquid in a rectangular domain is considered as shown in fig. 4.1(a). The bubble is assumed to be circular initially with a radius of R = 0.5 in the 2 x 8 rectangular domain. The simulation is carried out on a 66 x 258 grid. Tests have shown that with finer grids, better interface resolutions are achieved. Conversely, shock structures and shock speeds are not so much affected by increasing grid resolution [5].

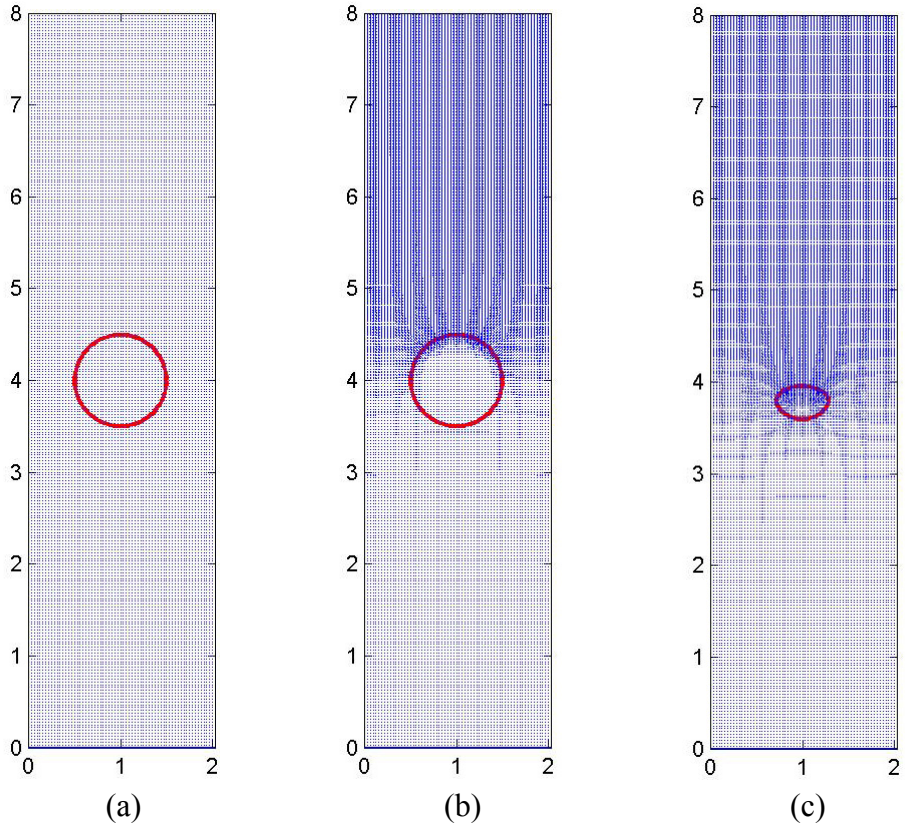

Figure 4.1: Solution of a single vapor bubble in a two dimensional, rectangular domain by front tracking/finite difference method†.

In fig. 4.1(a)-(c), the propagation of a pressure jump in a bubbly liquid is presented. The surface tension is set equal to zero and the pressure inside the bubble is kept

† A pressure jump of Δp = 0.4 is applied continuously at the top. The densities and viscosities are as follows: ρ_l = 2.5, ρ_b = 0.25, μ_l = 0.07, μ_b = 0.007 with subscript "l" denoting liquid and "b" denoting the gas inside the bubble. The bubble is initially at rest with initial radius R = 0.5 (corresponding to Re = 28.57) (a) Initial configuration of the bubble at t = 0 with initial radius R = 0.5. (b) The pressure jump immediately reaches the bubble passing through incompressible zone. The snapshot is taken at t = 0.1 . (c) The bubble collapses as the pressure wave passes by at t = 4 (darker areas in (b) and (c) show higher pressure zones).

constant (vapor bubble). As the pressure jump reaches the bubble, it starts to collapse in a deformed shape. As the bubble collapses, a jet flow occurs from the top to the bottom surface of the bubble. After the shock wave passes by, the bubble collapses completely and vanishes.

4.1.2 Shock Propagation in Bubbly Liquids Containing Vapor Bubbles

The problem is simulated for a bubbly liquid, containing initially 12 circular bubbles at rest with radius $R = 0.3$. The domain is a 2 x 8 rectangular domain and is resolved by 66 x 258 grid points. Other conditions like densities, viscosities and pressure jump are the same as in the single bubble case above.

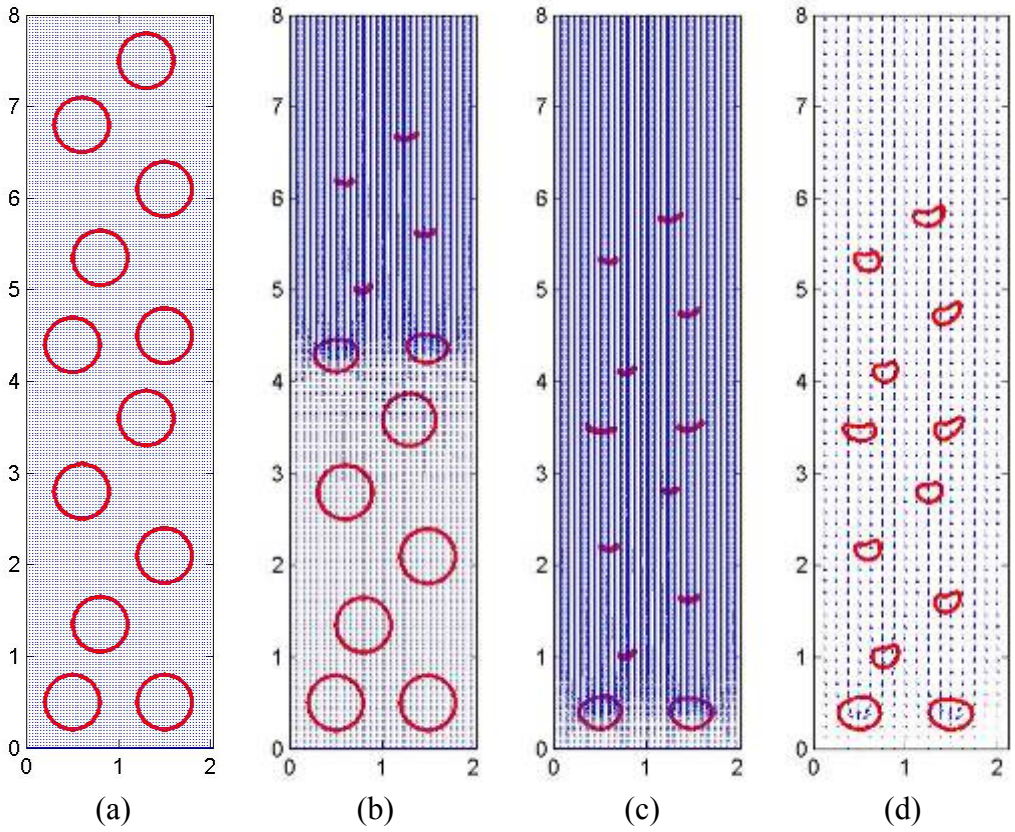

Figure 4.2: Solution for the propagation of nonlinear pressure waves in a 2D rectangular domain of a bubbly mixture containing 12 vapor bubbles by front tracking/finite difference method†.

† A pressure jump of $\Delta p = 0.4$ is applied continuously at the top. The densities and viscosities are as follows: $\rho_l = 2.5$, $\rho_b = 0.25$, $\mu_l = 0.07$, $\mu_b = 0.007$ with subscript "l" denoting liquid and "b" denoting the gas inside the bubbles. The bubbles are initially uniformly distributed with initial radius $R = 0.3$ (corresponding to Re=17.14). (a) Initial configuration of bubbles at t=0.0 in a 66x258 rectangular grid (b) t=4.0 in a 66x258 rectangular grid (c) t=8.0 in a 66x258 rectangular grid (d) t=8.0 in a coarser, 18x66 rectangular grid. The bubbles are resolved up to smaller volumes during collapse in fine grids. The processing time is measured in a 1700 MHz CPU for simulations in 18x66, 34x130 and 66x258 grids. The CPU time for the 18x66 grid resolution is 45 seconds. For the 34x130 grid resolution, the CPU time is 17 minutes 43 seconds while it is equal to 3 hours 33 minutes 1 second for the 66x258 grid resolution (darker areas in (b) and (c) show higher pressure zones).

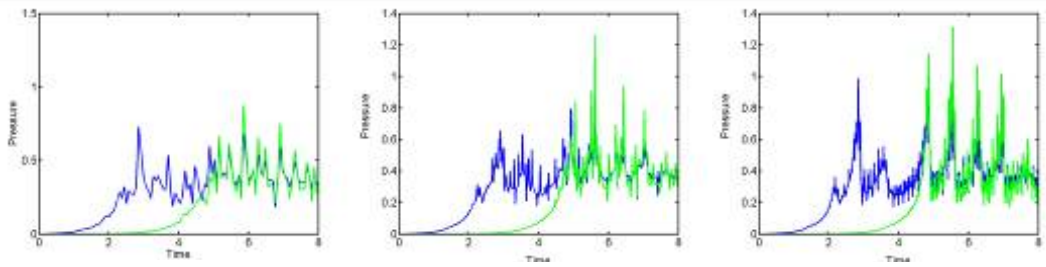

(a) (b) (c)

Figure 4.3: Pressure distributions for the propagation of nonlinear pressure waves in a 2D rectangular domain of a bubbly mixture containing 12 vapor bubbles†.

Figures 4.2(a)-(c) show the results of the simulations for the propagation of the shock in the 2 x 8 rectangular domain with a grid resolution of 66 x 258 at different times. Figure 4.2(d) shows the result of the same simulations in a coarser grid. It is obvious that the bubbles are not as well resolved as the ones in finer grids. When the collapsed bubbles are compared with those of fig. 4.2(c), it is easily observed that finer grids lead to better bubble resolutions. The bubbles can be tracked until very small volumes are reached in finer grids.

The green lines in fig. 4.3 show the pressure distribution at x = 0, y = 4. Similarly the blue lines in the same figures show the pressure distribution at x = 0, y = 6. Using the time evolution of constant pressure rises at the given stations, the mean propagation speed from the simulations can be found by dividing the distance traveled by the average time. The propagation speeds from the simulations are then found as 0.9128, 0.8928 and 0.8808 for 18 x 66, 34 x 130 and 66 x 258 grid resolutions, respectively. For a bubbly liquid containing 12 bubbles, each of radius R = 0.3, in the 2 x 8 rectangular domain, the void fractions are $\beta_0 = 0.2121$ and $\beta_1 = 0.0$, respectively. The propagation speed for the nonlinear pressure wave is then evaluated by eq. (2.5) to give $U_s = 0.9784$ for the pressure jump $\Delta p = 0.4$ and liquid density $\rho_l = 2.5$. The shock speeds obtained from the simulations are in agreement within 10% error with that of the of one-dimensional homogeneous bubbly liquid theory ($U_s = 0.9784$ given by eq.(2.5)). As can be seen, increasing grid resolution does not contribute to the accuracy of the shock speed as much as it does for resolving bubble/liquid interfaces.

† Pressure distributions at dimensionless locations y=4 (green) and y=6 (blue) along x=0 line. The propagation velocity is found as (a) 0.9128 for the 18x66 grid resolution, (b) 0.8928 for the 34x130 resolution and (c) 0.8808 for the 66x258 grid resolution. The fluctuations are better resolved as the grid resolution is increased.

4.1.3 Collapse of a Single Gas Bubble

In this section, a gas bubble is considered. The pressure of the gas is assumed to change isothermally with $\gamma = 1$ in eq. (3.3).

The pressure no longer remains constant when the bubble starts to collapse. During the collapse, the volume of the bubble decreases and this leads to a pressure increase inside the bubble. After some time the pressure may reach a value greater than the liquid pressure so that bubble growth may take place. The pressure decreases inside the bubble when the bubble gets larger, and when the pressure reaches a smaller value than the surrounding pressure, bubble collapse occurs again. This is an oscillating behavior.

In fig. 4.4, the computation is carried out in a 2 x 8 rectangular domain with a resolution of 34 x 130 grid points for a single gas bubble of radius $R = 0.5$. The density, viscosity and pressure jump values are the same as in the case of a vapor bubble and the surface tension is neglected.

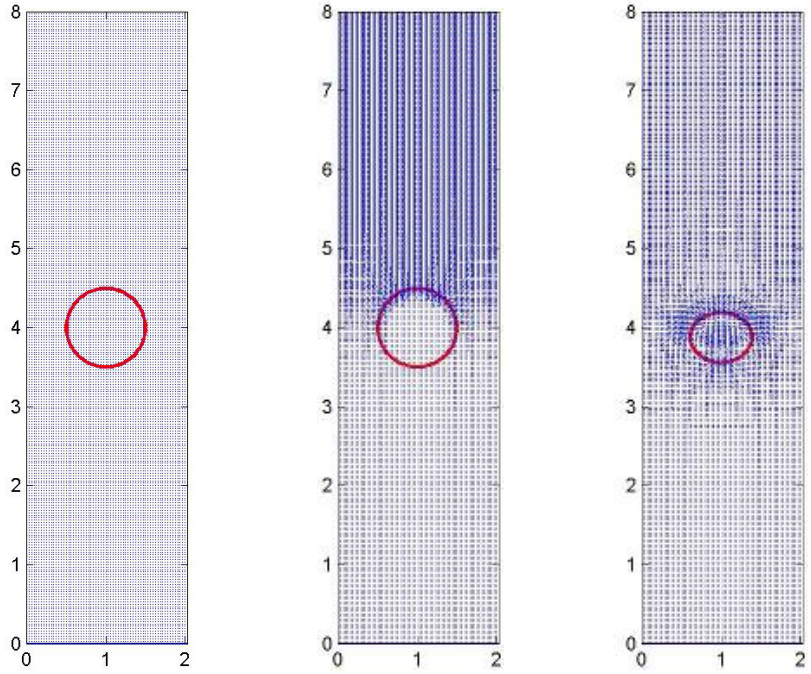

Figure 4.4: Solution of a single gas bubble in a two dimensional, rectangular domain by front tracking/finite difference method†.

† A pressure jump of $\Delta p = 0.4$ is applied continuously at the top. The densities and viscosities are as follows: $\rho_l = 2.5$, $\rho_b = 0.25$, $\mu_l = 0.07$, $\mu_b = 0.007$ with subscript "l" denoting liquid and "b" denoting the gas inside the bubble. The bubble is initially at rest with initial radius $R = 0.5$ (corresponding to $Re = 28.57$) (a) The bubble is at rest at $t = 0$. (b) The pressure jump immediately reaches the top of the bubble surface at t=0.1 . (c) Bubble collapses and pressure inside the bubble increases obeying isothermal law as the pressure wave passes by at $t = 4.5$ (darker areas in (b) and (c) show higher pressure zones).

As the pressure wave reaches the bubble, the bubble starts collapsing like the vapor bubble above. However, the pressure inside the bubble increases after some time and the collapse rate decreases. Finally, it may reach values greater than the surrounding liquid pressure resulting in bubble oscillations.

4.1.4 Shock Propagation in Bubbly Liquids Containing Gas Bubbles

The simulation is carried out for 12 bubbles in the same rectangular domain. The initial and boundary conditions are the same as for the simulation of 12 vapor bubbles given above.

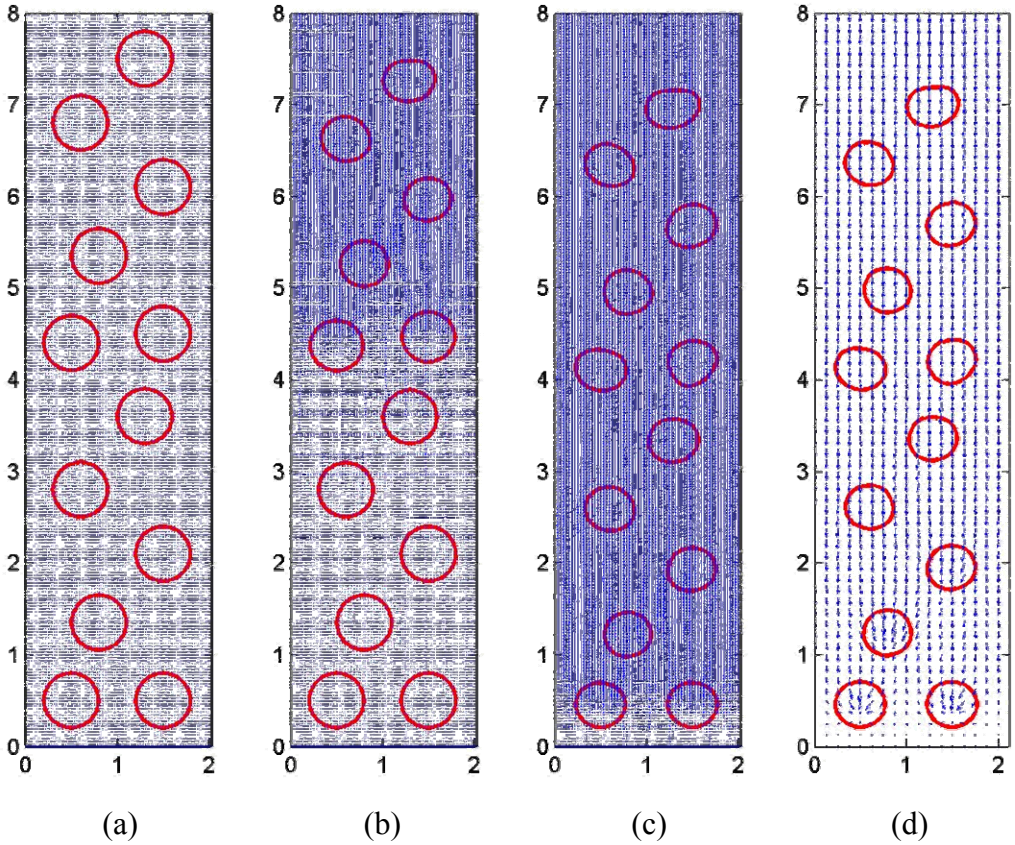

Figure 4.5: Solution for the propagation of nonlinear pressure waves in a 2D rectangular domain of a bubbly mixture containing 12 gas bubbles by front tracking/finite difference method†.

† A pressure jump of $\Delta p = 0.4$ is applied continuously at the top. The densities and viscosities are as follows: $\rho_l = 2.5$, $\rho_b = 0.25$, $\mu_l = 0.07$, $\mu_b = 0.007$ with subscript "l" denoting liquid and "b" denoting the gas inside the bubbles. The bubbles are initially uniformly distributed with initial radius $R = 0.3$ (corresponding to $Re = 17.14$). (a) Initial configuration of bubbles at t=0.0 in a 66x258 rectangular grid (b) the pressure wave passes by at t=2.0 in the 66x258 grid (c) at t=4.5 in the 66x258 grid and (d) at t=4.5 in a coarser, 18x66 rectangular grid. Although the bubbles are better resolved during collapse in fine grids, there is not any significant change in bubble shapes like it has been in vapor bubbles. The reason is that the bubbles do not collapse completely. Bubbles are better resolved in finer grids. The processing time is measured in a 1700 MHz CPU for simulations in the 18x66, 34x130 and 66x258 grids. The CPU time for 18x66 grid resolution is 25 seconds. For 34x130 resolution the CPU time is 6 minutes 50 seconds while it is equal to 1 hour 58 minutes 20 seconds for the 66x258 grid resolution. (darker areas in (b) and (c) show higher pressure zones.)

Figures 4.5(a)-(c) show the results of the simulations for the propagation of the shock in the 2 x 8 rectangular domain with a grid resolution of 66 x 258 at different times. Figure 4.5(d) shows the result of the same simulations in a coarser grid. Now the bubble resolutions are not very different. The reason is that the bubbles do not collapse completely. The isothermal pressure increase keeps the bubbles within a size that can be resolved in coarser grids.

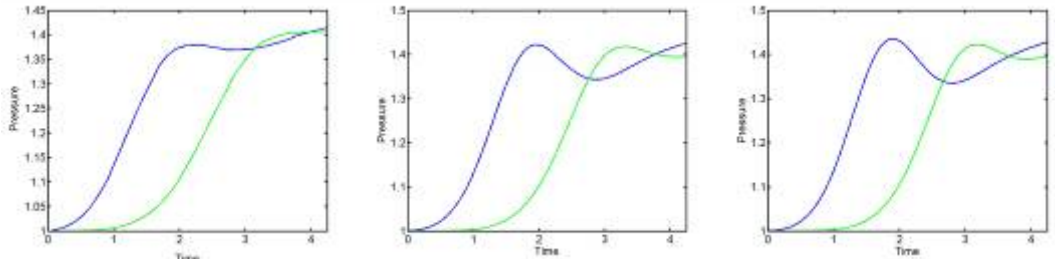

(a) (b) (c)

Figure 4.6: Pressure distributions for the propagation of nonlinear pressure waves in a 2D rectangular domain of a bubbly mixture containing 12 gas bubbles†.

The green line in fig. 4.6, show the pressure distribution at x = 0, y = 4. Similarly the blue line in the same figure shows the pressure distribution at x = 0, y = 6. The propagation speed results from the simulations are equal to 1.7340, 1.7504 and 1.7606, respectively, for the 18 x 66, 34 x 130 and 66 x 258 grids. These speeds are found using the procedure outlined above for vapor bubbles. For a bubbly liquid containing 12 bubbles, each of radius $R = 0.3$ in a 2 x 8 rectangular domain, the void fractions are as follows: $\beta_0 = 0.2121$ and $\beta_1 = 0.1515$. The shock speed for $\Delta p = 0.4$ and $\rho_l = 2.5$ is then evaluated as $U_s = 1.6862$ using eq. (2.5). The shock speed results of the simulations are in agreement within 5% error with the result of one-dimensional homogeneous bubbly liquid theory ($U_s = 1.6862$ by eq.(2.5)). Consequently, grid resolution, as in the case of vapor bubbles, is not very significant in evaluating shock speeds.

† Pressure distributions at dimensionless locations y=4 (green) and y=6 (blue) along x=0 line. The propagation velocity is found as (a) 1.7340 for the 18x66 grid resolution, (b) 1.7504 for the 34x130 grid resolution and (c) 1.7606 for the 66x258 grid resolution. The pressure fluctuations are better resolved in the finer grid.

4.2 Three-Dimensional Simulations for Vapor Bubbles

DNS of shock propagation in a bubbly liquid in a three dimensional rectangular domain is considered. A 1 x 1 x 4 rectangular domain is represented, respectively, using 18 x 18 x 66, 34 x 34 x 130 and 66 x 66 x 258 grid points. There are 16 spherical vapor bubbles, each of initial radius $R = 0.25$, in the 3D rectangular domain.

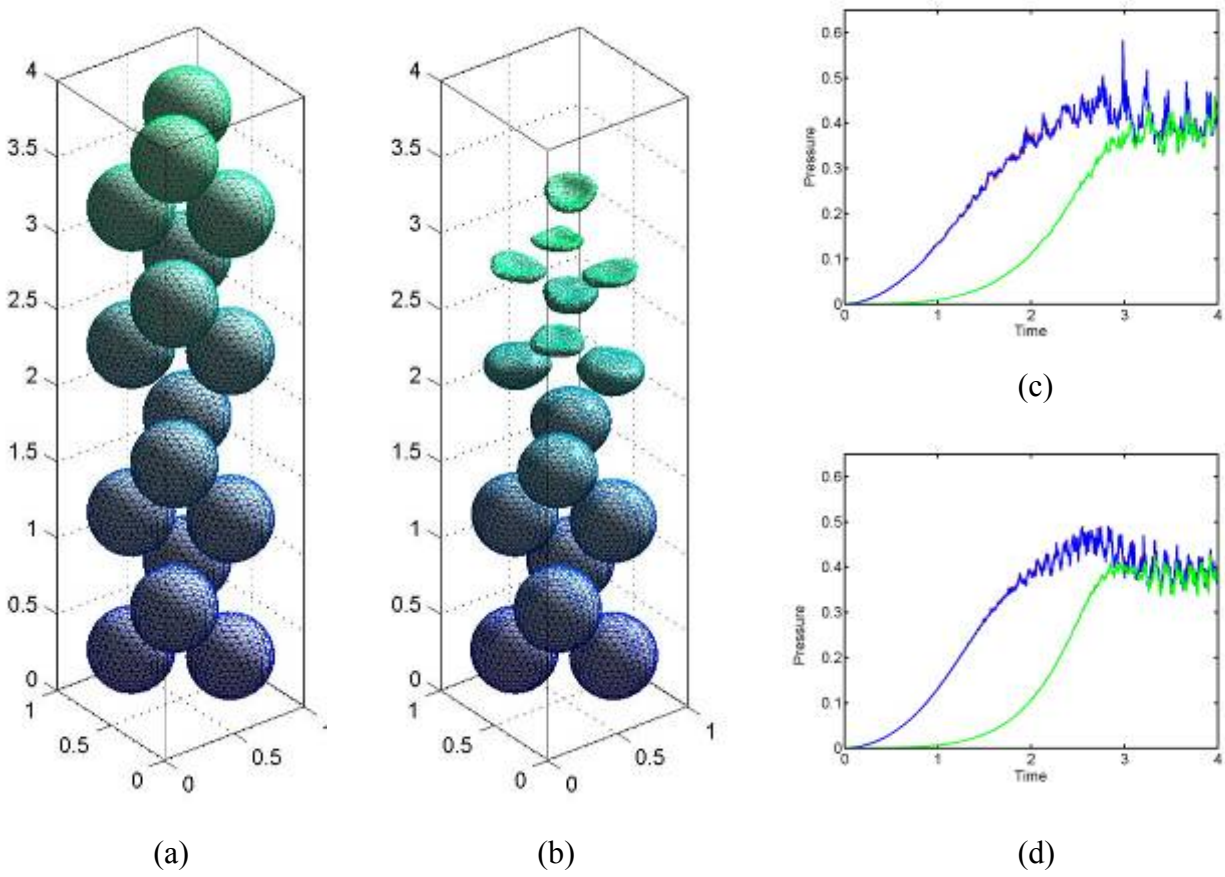

(a) (b) (c) (d)

Figure 4.7: Results of shock propagation in a bubbly mixture containing 16 spherical vapor bubbles†.

The pressure inside the bubbles is kept constant. A pressure jump $\Delta p = 0.4$ is imposed at the top boundary. The simulations show that bubble shapes do not remain spherical during the propagation of the pressure wave.

† The pressure jump $\Delta p = 0.4$ is applied at the top surface of the domain continuously. The bubbles are initially uniformly distributed with initial radius $R = 0.25$ (corresponding to $Re = 10$). (a) Snapshot at $t = 0$. (b) The collapse of the bubbles with deformed shapes at $t = 2.5$ (c) The pressure distributions at z = 2 (green line) and z = 3 (blue line) along the z axis using 18 x 18 x 66 resolution. (d) The pressure distributions at z = 2 (green line) and z = 3 (blue line) along the z axis using 34 x 34 x 130 resolution.

A wall boundary condition is imposed at the bottom of the domain with no liquid outflow. The lateral directions are simulated under the assumption of periodic boundaries. Figures 4.7 (a)-(b) show the initial (t=0) configuration and the configuration at a later time (t=3.5) as the shock propagates, exhibiting the characteristics of one-dimensional wave propagation in bubbly mixtures. The green lines in fig 4.7(c)-(d) show the pressure distribution at x = 0, y = 0, z = 2. Similarly the blue lines in the same figures show the pressure distribution at x = 0, y = 0, z = 3. Using the average arrival time for a constant pressure rise to reach a given station, the mean propagation speed from the simulations can be found as above, by dividing the distance traveled by the average time. Results from the different grid sizes seem to agree at a glance. For the coarsest grid, the pressure fluctuations are larger. The simulations until dimensionless time t = 4 for the 18 x 18 x 66 domain took 1 hour 6 minutes and 57 seconds on a 1700 MHz CPU. The mean propagation speed from the simulations is found to be U_s = 0.9538. The same simulations lasted 45 hours 30 minutes and 33 seconds on the 34 x 34 x 130 grid on the same CPU. The result for the propagation speed still did not change. It is calculated as U_s = 0.9547 . The result for the shock speed is quite in agreement with the value U_s = 0.9099 of one-dimensional homogeneous bubbly liquid theory, evaluated from eq. (2.5). Except for the very coarse 18 x 18 x 66 grid, there is no special need to make the grid finer. The more points the grid includes, the better the bubbles are resolved. Better resolution of bubbles is essential for interfacial phenomena like surface tension.

5. CONCLUSION

The present simulations for the propagation of shock waves in bubbly liquids show that one-dimensional homogeneous bubbly flow model is still successful for void fractions up to 15% to 25% [5]. This result is achieved for incompressible liquids and for constant pressure or isothermal pressure changes inside the bubbles. On the other hand, fluctuations of pressure waves show that shock propagation for the domains considered is yet unsteady. The pressure fluctuations being stronger for vapor bubbles seem responsible for the difference of shock speeds between vapor bubble simulations and classical theory.

Grid convergence analyses of front tracking finite difference method are made for bubbly liquids containing vapor bubbles in 2D and 3D, and for bubbly liquids containing gas bubbles in 2D. The grid convergence analyses show that grid resolution doesn't contribute to the results of propagation speeds remarkably. On the other hand, for vapor bubbles, the grid resolution is important in resolving bubble/liquid interfaces. In this case, bubbles can be resolved until two opposite surfaces touch each other. In addition pressure fluctuations are better resolved in finer grids, especially for vapor bubbles. Vapor bubbles are more sensitive to grid resolution both for resolving bubble/liquid interfaces and pressure fluctuations.

In order to make a comparison of results with experiments [4], thermal relaxation effects should also be considered. Addition of thermal damping requires that energy equations be solved coupled with the Navier Stokes equations. Furthermore, liquid compressibility can be brought up for more realistic analysis. The investigations of these effects are left out for future investigations.

REFERENCES

[1] **Watanabe, M. and Prosperetti, A.,** 1994. Shock waves in dilute bubbly liquids, *J. Fluid Mech.*, **66**, 115-143.

[2] **Beylich, A.E. and Gülhan, A.,** 1990. On the structure of nonlinear waves in liquids with gas bubbles, *Phys. Fluids A*, **2**, 1412-1428.

[3] **Noordzij, L. and van Wijngaarden, L.,** 1974. Relaxation effects caused by relative motion on shock waves in gas-bubble/liquid mixtures, *J. Fluid Mech*., **66**, 115-43.

[4] **Kameda, M., Shimaura, N., Higashino, F. and Matsumoto, Y.,** 1998. Shock waves in a uniform bubbly flow, *Phys. Fluids*, **10**, 2661-2668.

[5] **Delale, C.F., Nas, S. and Tryggvason, G.**, 2005. Direct numerical simulations of shock propagation in bubbly liquids, *Phys. Fluids*, **17**, 121705-1-4.

[6] **Tryggvason, G., Bunner, B., Esmaeeli, A., Juric, D., Al Rawahi, N., Tauber, N.W., Hans, J., Nas, S. and Jan, Y.J.,** 2001. A front tracking method for the computations of multiphase flow, *J. Comput. Phys*, **169**, 708-759.

[7] **Leighton, T.G.,** 1994. The Acoustic Bubble, Academic Press, London.

[8] **Brennen, C.E.,** 2005. Fundamentals of Multiphase Flows, Cambridge University Press, London.

[9] **Fox, F.E., Curley, S.R. and Larson, G.S.,** 1955. Phase velocity and absorption measurements in water containing air bubbles, *J. Acoust. Soc. Am*., **27**, 534-539.

CURRICULUM VITAE

Sarper Arün was born in Istanbul in June 17th, 1981. He graduated from Hayrullah Kefoğlu High School in Istanbul with honors and first rank in 1999. In the same year, he entered the Aeronautical Engineering Department of the Faculty of Aeronautics and Astronautics at Istanbul Technical University. He graduated from the same department in 2003. He has been studying towards his master degree in the same department since 2003.